Enhanced early photon optical projection tomography system for mesoscopic imaging of thick tissues

L. Sinha,[1,2a)] W. Zhou,[2] D. Walus,[1] J. G. Brankov,[2] and K. M. Tichauer[1,b)]

[1]*Department of Biomedical Engineering, Illinois Institute of Technology, Chicago, Illinois 60616, USA*
[2]*Department of Electrical and Computer Engineering, Illinois Institute of Technology, Chicago, Illinois 60616, USA*

(Received XXXXX; accepted XXXXX; published online XXXXX)
(Dates appearing here are provided by the Editorial Office)

This document gives formatting instructions for authors preparing a Note for publication in *Review of Scientific Instruments*. Authors must follow the instructions given in this document; it should be used as an instruction set. **Note: RSI Notes do not contain headings. The headings used in this sample are to be used as a navigational tool and aid in readability.** All files MUST be submitted through the online system at: **http://rsi.peerx-press.org**.

INTRODUCTION

Optical tomography

Today cancer is known to be heterogeneous in nature, showing both intra as well as inter-tumor heterogeneity[1]. Cancer continues to be the second leading cause of death in the world with one in two individuals suffering from some form of cancer within their lifetimes[2]. This necessitates development of imaging methodologies that can achieve resolution at the molecular level such that these heterogeneities can be observable and appropriate drug can be administered. Highly resolved images of cancerous tissue can be obtained *ex-vivo* by the process of histopathology, during which the tissue loses its structure and are cut into few microns thick slices. Imaging modalities like single photon emission computed tomography (SPECT) or positron emission tomography (PET) can achieve very high-resolution images of the entire body but they suffer from inherent disadvantages of using radiation as a means of imaging [3] [4]. In addition to the expensive instrument required for imaging, the patient is also exposed to ionizing radiation that has its own set of adverse effects[3]. Near infrared light penetrates quite deep through human tissue compared to visible light and this was utilized in case of optical imaging[5] [6]. Optical tomography is a non-invasive technique to image human tissue. A trade off exists i.e. even though radiation is absent in case of optical tomography, it fails to achieve resolution comparable to SPECT or PET due to scattering of light in diffuse regime.

The problem of scattering in tissue

Scattering has always been a major hindrance when using optical tomography in tissue. Penetration of light through tissue depends on several parameters like intensity and wavelength of light, tissue compression, tissue properties like pigmentation, structure, hydration, composition, only to name a few. Broadly, optical scattering occurs when there is a refractive index mismatch between the particle and the surrounding medium or there is a continuous fluctuation in the refractive index of a medium. There can be two kinds of scattering in case of biological tissue - Rayleigh and Mie scattering. While Rayleigh scattering refers to scattering due to particles that are much smaller than the wavelength of light, Mie scattering happens when the mass density fluctuation is comparable to or larger than the wavelength[7]. Scattering in tissue is a major obstacle in case of optical tomography.

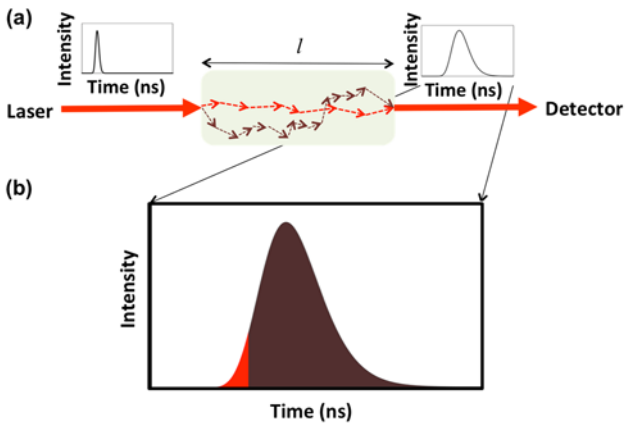

Fig 1. The fate of photons as they travel through the tissue of length *l*. (a) The pulse broadening is demonstrated in time domain with respect to their normalized intensities. The bright red arrows indicate the path taken by few of the

photons that encounters minimal scatter while most of the photons scatter randomly in the tissue and reach the detector (blackened red). (b) The pulse spread function is shown color-coded with the arrival time of the photons corresponding to the path taken by them. The bright red ones taking a shorter path arrive earliest while the others arrive late.

The optical properties of tissue are described mainly by four quantities - μ_a (the absorption coefficient), μ_s (the scattering coefficient), n (refractive index) and g (anisotropy of scatter). Propagation of light through tissue can be described by the radiative transfer equation, which demonstrates the spreading of the pulse in time domain as it moves through the tissue. Interaction of photons with tissue makes them scatter in different directions thereby varying the time of arrival of the photons at the detector that explains the temporal broadening of a narrow light pulse from the source as it reaches the detector passing through the tissue (**Fig 1**). As the photons scatter more, they get diffused more into the tissue and continue to lose information content of the image causing increase in blurring in image domain. However, while most of the photons experience high amount of scattering in the tissue some of them scatter less and travel almost straight through the tissue. These are the early arriving photons at the detector which has more information content compared to the late arriving diffused ones (**refer optics letter**).

Early Photon tomography

While travelling through the tissue some of the photons undergo no scattering and remain on the optical axis and reach the detector at the earliest. These are known as the ballistic photons. Those, which experience minimum scattering so much so that they remain near the optical axis and reach the detector, are known as quasi-ballistic photons. Due to the above-mentioned reason the ballistic ones arrive first at the detector followed by the quasi-ballistic ones, which is then followed by the scattered or diffused photons (**Fig 1b**). But with increase in the tissue thickness, the probability of getting scattered increases therefore decreases the probability of receiving ballistic photons, but only a few photons that get scattered in the forward direction reach the detector earliest. These early arriving photons have followed the direct path and so have suffered the least amount of scattering in the tissue. Early photon tomography makes use of these early arriving photons to obtain high-resolution images through the tissues[8, 9]. Early photon tomography makes high-resolution optical tomography possible in tissues by collecting only the early arriving photons and dumping the late arriving scattered ones. In the past, mainly two methods have been adopted to obtain the earliest arriving photons - gated early photon tomography and single photon counting early photon tomography.

In case of gated early photon imaging an intensifier or an ultrafast optical shutter was used on the detector with a repetition rate triggered by the laser to enable the detector to receive the earliest arriving photons while rejecting the late arriving ones[9]. Gated early photon detection was also achieved by delaying the input laser signal by a delay line and combining it with the temporally spread laser pulse (as it travels through the tissue) with the help of β-barium-borate (BBO) crystal[10]. Improved resolution and image quality was obtained by using such gated method.

The major hindrance in the path of obtaining higher resolution in such an approach was the large shutter gate size (200 ps but **100 fs for Fieramonti**) and presence of timing uncertainty. Therefore single photon counting early photon tomography followed suit[11]. Time correlated single photon counting (TCSPC) module was used where single photon arrival time could be determined[8]. The timing uncertainty in case of the gated approach could be avoided by time stamping each photon which was achieved by the module by simultaneously receiving the synchronization signal from the laser and the single photon detection signal from the single photon detector. The arrival time could then be used as the determining factor for the collection of early arriving photons while rejecting the late arriving ones [11]. The most commonly used single photon detectors are single photon photomultiplier tube (PMT) and single photon avalanche diode (SPAD). A comparative study can be found in the literature[12]. This approach of using time correlated single photon counting is able to achieve early arriving photons which are sparingly scattered.

This paper discusses in details a novel approach of receiving the earliest of the arriving photons by pushing the limits of the single photon detector. Saturating the detector and making it to work in the dead time regime can enhance the detection of early photons.

Deadtime enhanced early photon detection (DEEP)

After detection of a photon the time taken by the detector, during which it remains inactivate, to get prepared to record another event is known as the dead time of the detector[13]. The total dead time of a system is the combined dead time of the detector (SPAD) along with the dead time of the TCSPC module. A SPAD was selected for the purpose because of its robustness compared to a PMT as discussed. While a PMT can get permanently damaged at very high intensity a SPAD will go into its dead time mode and again re-activate itself after the dead time is over. This dead time as can be observed occurs only after the detection of one photon. So, if the laser is powerful enough with a pulse repetition frequency less than the inverse of the dead time, every photon that the detector detects per pulse is the earliest arriving one and the late arriving ones are therefore rejected as they fall in the dead time regime. This novel approach heightens the detection of the very early arriving photons at the expense of late

arriving scattered ones (**Fig 2**). The probability of detection as can be observed is 1 initially, detecting early photons, but decreases to almost 0 with increased power i.e. more dead time effect affecting the later gates.

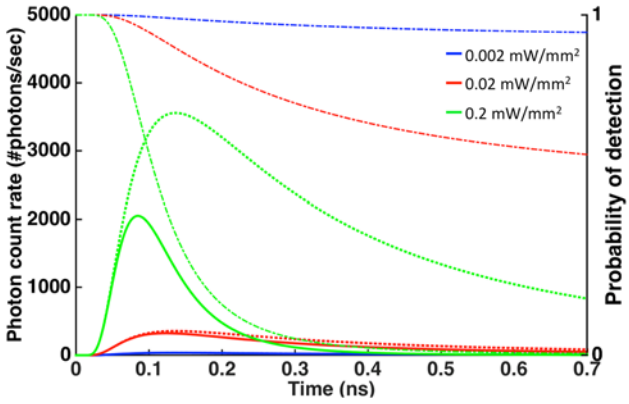

Fig 2. Simulation study demonstrating the enhancement in early photon detection with increased dead time effect. While the blue curve depicts a curve without saturation (0.002 mW/mm^2), green and red ones (0.2 and 0.02 mW/mm^2) denote curves with increased power i.e. increase in saturation effect. The dashed ones are the TPSFs which would have been obtained without any saturation at the detector while the bold lines are the ones which are actually obtained with the dead time effect. The corresponding dashed and dotted lines denote the probability of detection of the photons at the detector.

PRINCIPLES OF DEEP

Selection of frequency

The combined dead time of the detector and the TCSPC is 77 ns. If the pulse period of the laser is less than the dead time then a photon from one pulse reaching the detector at the end of the dead time may be detected as a photon coming from another pulse. To avoid this issue the pulse repetition should be such that the pulse period is greater than 77 ns (**refer**). Moreover another significant effect when dealing with high laser power is afterpulsing observed at the detector. Afterpulsing is a phenomenon which generates a second signal following the first real signal due to embedded electrons (**refer**). This can affect the reading as a photon is detected by the detector due to afterpulsing even though no real photon arrives at the detector. This can cause false photon detection and erroneous results. Therefore the effect of it should be minimized. In SPAD the afterpulse has a very gradual slope in microseconds and so the pulse period should be such that even if the afterpulse is detected, as it is difficult to avoid at high laser intensity, can be accounted for. Therefore a pulse repetition of 5 MHz was selected; having a period of 200 ns, such that even if the detector enters into its dead time mode for 77 ns after detection of first photon and the afterpulse affects the late arriving scattered photons after the dead time is over can gradually decrease to maintain a constant background signal that can be thresholded out.

SYSTEM DESIGN

System schematic

The system schematic is demonstrated in **fig. 3**. A **785nm laser** was used as the light source. Discuss about the laser.

The collimated light from the laser is then sent through a neutral density filter that can be varied from 0.5-4 OD **(**Thorlabs, Newton, NJ**)**. This filter can be used to maintain the power of the laser and can be varied such that the detector can run at both dead time regime as well as normal mode. A high OD selection will have a lower transmission and hence can make the detector work normally without dead time effect) without changing any other setting. Laser power was monitored with the help of a power meter (S120C, Thorlabs).

The laser light is then filtered by a clean-up filter or excitation filter (Chroma Technology Corp., bellow Falls, VT) that transmits a very narrow range of wavelengths near the laser wavelength while blocking other wavelength light to minimize background signal and other artifacts.

The collimated light then needs to be focused on the object. This is performed by a 300 mm lens **(**Thorlabs, Newton, NJ**)** placed after the excitation filter. The 300 mm lens was selected as simulation studies demonstrated (**Fig. 4**) that a 50um spot size could be achieved at the object with a beam waist large enough such that it is not converging very steeply at the object. If they had converged very steeply all the photons hitting the object will be oriented differently while if the waist is large enough most of them will be oriented in the same direction. The simulation study was performed using ray tracing matrices **(refer paper) since the light emitted from the laser is Gaussian in nature with a initial waist (w0) of 0.7 mm in the x axis and 2 mm in the y axis**. When the beam passes through a lens the following equation was used to trace the ray

$$\begin{bmatrix} x' \\ \theta' \end{bmatrix} = \begin{bmatrix} 1 & d \\ -\frac{1}{f} & 1-\frac{d}{f} \end{bmatrix} \begin{bmatrix} x \\ \theta \end{bmatrix} \quad (1)$$

where x, θ and x', θ' are the initial and final position and angle of the beam respectively; d is the distance between the two objects and f is the focal length of the lens in the path [14]. An infinite focal length was considered for the filters. All the computations were done assuming the initial beam waist to be 2 mm. However the beam loses its Gaussian nature once it arrives at the object as they pass

through a diffusing medium. Thereafter the beam becomes a scattered one.

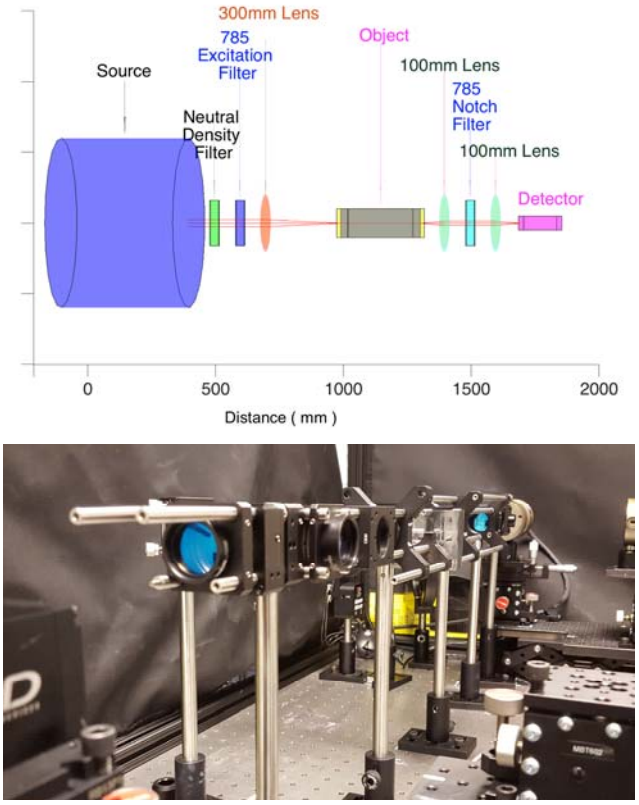

Fig 3. (a) Schematic of the system used. Five rays have been shown demonstrating the effect of each component as the rays propagate through. The lens are named with respect to their focal points (e.g. 300 mm lens means a lens with focal point at 300 mm). A fixed distance was maintained such that the front of the object was at the focal point from the 300 mm lens. Again 100 mm distance was maintained between the end of the object to the first 100 mm lens. Finally, the detector was placed at 100 from the second 100 mm lens. (b) Final system developed, shown from the detector side.

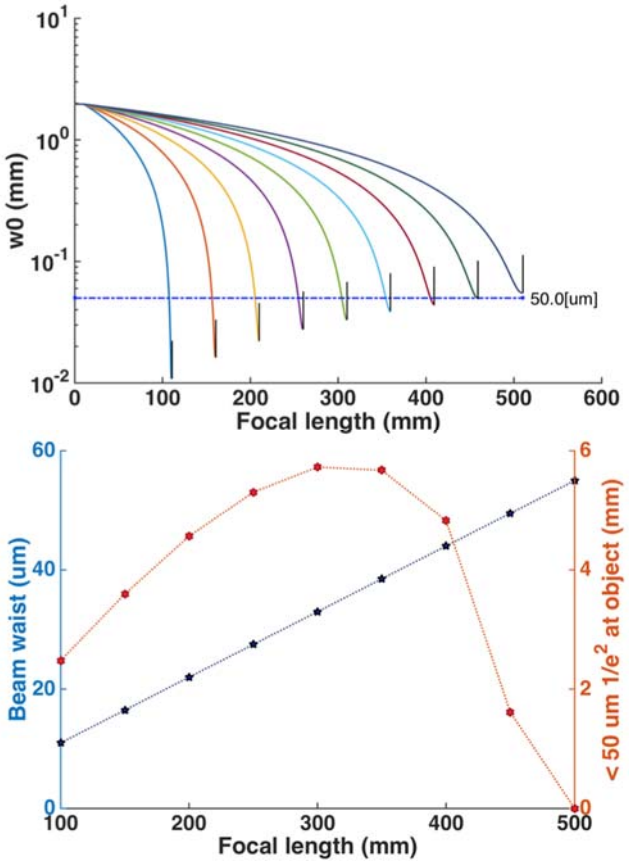

Fig 4. Simulated beam waist for selection of focal length of lens before the object. (a) The change in beam waist as different focal lengths of lens are selected is shown. (b) A comparison of beam waist and spot size at the object is shown with varying focal lengths. Since a large beam waist and a 50 um spot size is ideal the 300mm focal length lens was selected for our purpose.

The object consists of a 4mm thick 1% Intralipid® (Sigma-Aldrich, St. Louis, USA) and India ink (Winsor & Newton, London, UK) in water solution to match the optical properties of the tissue (μ_a = 0.02 mm^{-1} and μ_s‘ = 1 mm^{-1})[7] that is placed in a rotating chamber and immersed in a bath consisting of an optical matching fluid. The rotating chamber is fixed to a rotating stage (Thorlabs, Newton, NJ) which is connected to two linear stages (Thorlabs, Newton, NJ) that can move the chamber in horizontal and vertical directions helping in raster scanning the object.

The scattered beam coming off the object is refocused using a second lens pair. A 100 mm lens pair (Thorlabs, Newton, NJ) was selected which could focus a 50 μm spot size on the object to a 50 μm detector spot. Similar focal lengths were selected for the lens to maintain a magnification ratio of 1:1 from the object to the detector.

In between the two 100 mm lens the collimated light is made to pass through **an aperture** (Thorlabs, Newton, NJ) **to minimize the possibility of off-axis or unparallel light**. A comparison is provided **(fig)** the resolution obtained in the presence and absence of the aperture. **A**

785 notch filter (Chroma Technology Corp., bellow Falls, VT) **is also introduced in the path such that the high powered excitation light does not reach the detector while the emitted fluorescent light does**. While a cage system is used to guide the path of light, the filter is arranged such that it can be removed from the cage system as and when required. This filter is made removable such that the same setting can be used for both absorption based imaging (without filter) or fluorescence imaging (with filter).

The second 100 mm lens (Thorlabs, Newton, NJ) finally focuses the light onto the detector. The detector is a SPAD (PDM, PicoQuant) which is 50 μm x 50 μm in area. The NIM logic from the detector is used to obtain the detection pulse, which is given as input to the TCSPC module (**HydraHarp 400, PicoQuant**). The mechanism of hydraharp (**fig 5a**) can be described as a timer that determines the time interval between the laser signal and the time at which the photon hits the detector. It receives a synchronization (sync) signal from the laser at the same time as the pulse is generated and also receives the signal of the photon being detected at the detector from the SPAD. It then internally computes the arrival time of the photons i.e. the difference between the sync pulse and the detection pulse, and sends them to the computer for analysis after binning them in histograms. Even though the hydraharp is able to bin the arrival time of photons at 1 ps a **timing uncertainty of 25 ps is present in the detector**. However it can be shown that a temporal resolution is limited by the resolution at which the binning occurs. A simulation study shows that as the power is increased and the effect of dead time is enhanced the detection of early photons increases and is limited to a 1 ps bin which is due to the binning resolution. A simulated study was performed to determine the fate of binning as dead time increases for different binning resolution (**fig 5b**). On careful analysis it can be observed that with increase in binning resolution the desired value is reached much earlier compared to higher binning resolution. This shows that a smaller resolution if achievable can obtain much earlier photons even with dead time effects compared to the current 1 ps binning resolution. The higher photon counts of the 4 ps resolution might seem to achieve higher signal to noise ratio but it should also be kept in mind that it provides an integrated value over 4 ps while the others (1 ps and 1fs) have much smaller summation time and therefore have lesser photon count.

The dead time considered here can be of two types- extendable and non-extendable dead time[13].While the extendable dead time as the name suggests can extend when a second photon arrives in between the dead time after the detection of the first photon, in case of the non-extendable dead time the time for which the detector remains inactive is fixed after the detection of the first photon and does not change thereafter even if other photons hit the detector at that time. In case of the non-extendable dead time after the fixed period of dead time is over the detector is active again to detect the next photon while in case of non-extendable dead time the time for which it is dead increases proportionally with respect to the number of photons hitting the detector during the dead time. While the non-extendable dead time is mostly observed at lower powers (in the domain of our work), the probability of the occurrence of the extendable dead time is low and so can be ignored.

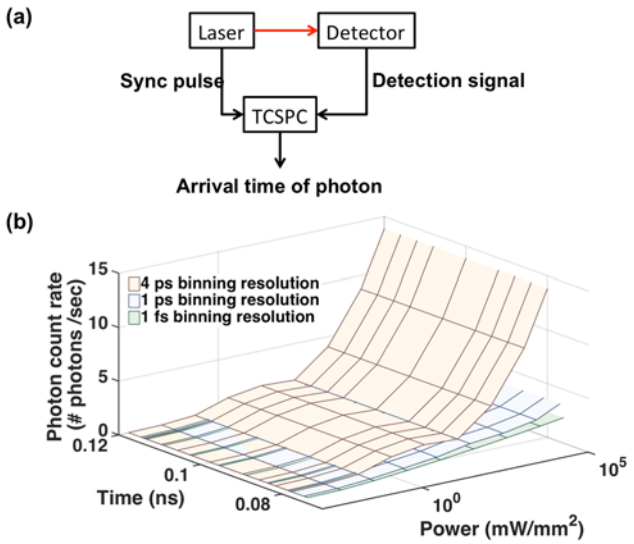

Fig 5. TCSPC mechanism and binning simulation. (a) A schematic demonstration of the mechanism of action of the TCSPC module. (b) A comparative study of the number of photons binned in a very early bin, which has 0.01% of the number of photons present in the peak of TPSF with different temporal binning resolutions as the power is increased.

Instrument response function

The instrument response function (IRF) of the system is obtained by making the laser light pass only through the bath filled with optical matching fluid and reach the detector (**fig. 6a**) . The IRF provides the response of the system in absence of any object in its path. The IRF of the system has a full width half maximum (FWHM) of 124 ps while the total spread is almost 1 ns. This 124 ps FWHM increases to nanoseconds when a thick tissue (2-4 mm) is placed in its path.

Stability

Linearity of early photon gates

An experimental study was performed to determine the linearity of the early time bins for different power. **Fig 6b** demonstrates that the linearity in each of the early time bin is maintained for at most three orders of magnitude while the zone of linearity shifts with different power for different time bins. After the phase of linearity there is a phase for which they are no more linear with increase in power the reason behind being the saturation effect creeps in at those time points decreasing the counts in those bins. Therefore the linearity decreases with increase in dead

time and finally when it is highly saturated (at higher power) the number of photons at the same bin drops because of the apparent shift of the TPSF as shown in **fig 2.**

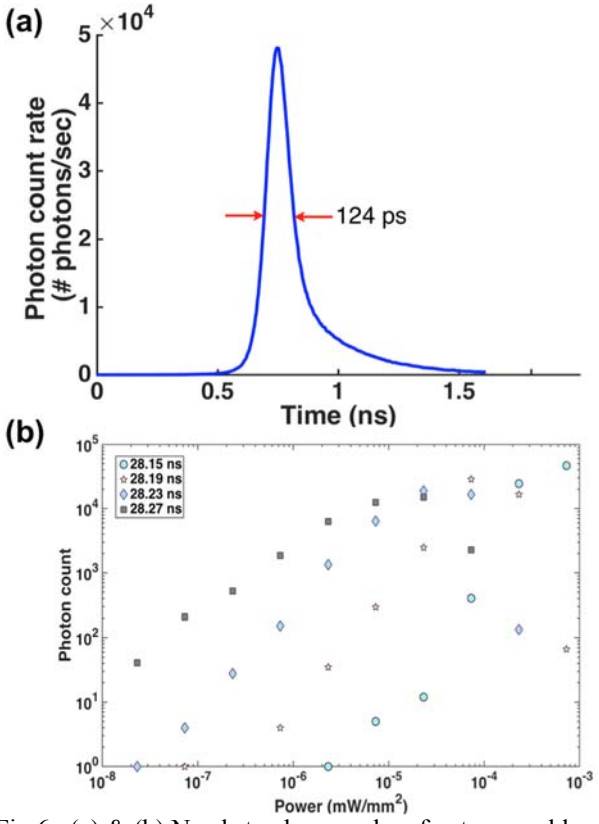

Fig 6. (a) & (b) Needs to change when femtosecond laser arrives

Afterpulsing (refer Picoquant)

Phantom experiments

Specimen preparation (phantom design)
%-Determination of the quantity of india ink required for obtaining signal (**Result figure**)
-Designing of mold for experiment
Result
Image reconstruction (**figure**) – 2D and 3D
If from actual phantom great else do with simulation reconstruction
Conclusion
Future impact in imaging world?
Acknowledgement

[1]D. L. Longo The New England journal of medicine **366,** (2012).
[2], (American Cancer Society, 2014).
[3]L. W. Dobrucki and A. J. Sinusas Nat Rev Cardiol **7,** (2010).
[4]S. R. Meikle, F. J. Beekman and S. E. Rose Drug Discov Today Technol **3,** (2006).
[5]W. M. Leevy, S. T. Gammon, H. Jiang, J. R. Johnson, D. J. Maxwell, E. N. Jackson, M. Marquez, D. Piwnica-Worms and B. D. Smith J Am Chem Soc **128,** (2006).
[6]U. Mahmood IEEE Eng Med Biol Mag **23,** (2004).
[7]S. L. Jacques Phys Med Biol **58,** (2013).
[8]M. J. Niedre, R. H. de Kleine, E. Aikawa, D. G. Kirsch, R. Weissleder and V. Ntziachristos Proceedings of the National Academy of Sciences of the United States of America **105,** (2008).
[9]G. M. Turner, G. Zacharakis, A. Soubret, J. Ripoll and V. Ntziachristos Optics letters **30,** (2005).
[10]L. Fieramonti, A. Bassi, E. A. Foglia, A. Pistocchi, C. D'Andrea, G. Valentini, R. Cubeddu, S. De Silvestri, G. Cerullo and F. Cotelli PloS one **7,** (2012).
[11]Y. Mu and M. Niedre Conf Proc IEEE Eng Med Biol Soc **2014,** (2014).
[12]Y. Mu and M. Niedre Biomedical optics express **6,** (2015).
[13]D. A. Gedcke, edited by O. A. N. AN57 (2001).
[14]H. Kogelnik and T. Li Applied optics **5,** (1966).